3D Modeling of a Planar Discharge in a CO_2 Laser Using a Multilevel Approach

J. Schüttler
Rofin-Sinar Laser GmbH, Berzeliusstraße 87, D-22113 Hamburg, Germany
j.schuettler@rofin.de

Abstract: The aim of the presented work is to simulate the properties and homogeneity of a planar gas discharge and the mutual interaction between the plasma and the driving radio frequency (RF) field in a complex 3D geometry. A fully coupled plasma and RF simulation in 3D is no feasible approach due to limited computational resources. Instead, the problem is partitioned into manageable tasks in a hierarchical way. First, the "zero dimensional" electron energy distribution function is calculated for the complex gas chemistry of the premixed laser gas, followed by a parametric 1D simulation of the discharge. By interpolating the U-I-curve of the 1D discharge and extracting characteristics like sheath thickness and carrier density, a surrogate model is built up for the electrical properties (e.g. impedance) of the plasma, which is then used as a (strongly nonlinear) material model in a 3D RF simulation of the complete CO_2-laser.

Keywords: laser, planar discharge, 3D simulation, plasma

1. Introduction

High power CO_2-lasers have been the workhorses for sheet metal cutting, welding and many more applications in materials processing during the past decades. Even though a significant replacement by fiber coupled lasers takes place, there are still many applications that benefit from the characteristics of CO_2-lasers with a high beam quality [1]. Therefore, further pushing the limits regarding power, stability, modulation etc. is in the focus of current development work.

CO_2-lasers are operated using a gas discharge to excite the CO_2 molecules in order to populate the upper lasing state. In Rofin's diffusion-cooled slab-laser design (Figure 1), the plasma is formed between two planar electrodes that simultaneously serve as an optical waveguide and provide a proper gas cooling [2].

Modeling the plasma behavior is essential for optimizing e.g. the homogeneity of the discharge, cooling design, gas dynamics inside the laser and

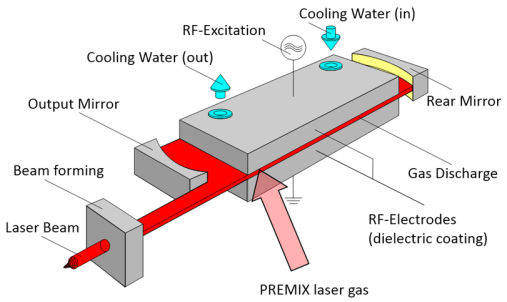

Figure 1. Working principle of a diffusion cooled CO_2-slab-laser (Rofin DC series).

the electrical properties of the system. Due to the complex pumping scheme of a CO_2-laser, many species and collisions have to be considered. CO_2-laser discharges have been studied in detail [3-5], but no directly transferable data is available for today's highly optimized laser gas mixtures.

The target of the work presented in this paper is to provide a model which allows to calculate the distribution of the driving RF field in a complex 3D geometry and its interaction with the plasma in regions where the electric field is sufficiently high to ignite a gas discharge.

Due to the wide range of time and length scales involved in this multiphysics problem, a directly coupled simulation of the microscopic plasma physics and the macroscopic RF distribution would result in a huge number of degrees of freedom as well as necessary time steps to find a (quasi-)stationary solution. Because of limitations in computational resources and time, this approach is obviously not feasible.

Instead, in the following sections a multilevel approach is presented, which allows to simulate the mutual coupling between the driving RF field and the self-consistent impedance of the plasma sheet by a separation of scales.

2. Overview of the Multilevel Approach

The hierarchical approach used in this work is motivated by some special properties of the CO_2-slab-laser, which are described in the following

section. Hereafter, the principle of the multilevel approach is presented.

2.1 CO_2-Slab-Laser Principle

The principal laser setup shown in figure 1 mainly consists of two planar electrodes facing each other with a gap of 1…2 mm. The dimensions of the electrodes are ranging from 1…2 m (length) and 0.2…0.3 m (width) depending on the laser model. The electrodes are typically coated with a thin dielectric layer for optical reasons as well as to stabilize the discharge.

The electrodes, laser mirrors and supporting structures (e.g. cooling pipes) are contained in a solid metal container ('recipient') which is evacuated and then filled with the premixed laser gas to a pressure of several 100 mbar. In the numerical model, the inner surface of the recipient bounds the calculation domain.

Most of the many parts inside the recipient have conducting surfaces, which influence the distribution of the RF field. Hence, to investigate the homogeneity of the discharge, it is not viable to simplify the resulting complex 3D structure.

2.2 Model Hierarchy

From the modeling point of view, the main advantage of the system under investigation is that the discharge volume is a thin slab. It is reasonable to assume that the electric field component normal (E_z) to the electrode surface is much larger than the tangential components (E_x, E_y), and that the variations of the electric field, temperature, pressure etc. are small in the tangential direction, at least on a length scale comparable to the electrode gap:

$$|E_z| \gg |E_x|, |E_y|$$
$$|\partial_{x,y}(E, p, T, \dots)| \ll |\partial_z(E, p, T, \dots)|$$

Therefore, a 1D-approximation for the gas discharge is valid in most regions of the electrode gap. Additionally, the plasma dynamics develop on a much faster timescale than the macroscopic parameters, such as pressure and temperature variations.

This allows to split the simulation into the following steps:

1) Calculation of the local plasma properties such as electron statistics, particle mobilities, collision rates in '0D' as a function of electron energy or reduced electric field,
2) Simulation of the discharge properties, such as thermal losses or electrical impedance in a 1D approximation of the discharge, and
3) Using the parametric dependencies of the (quasi-steady-state) discharge as surrogate material in large-scale 3D simulations of the RF properties.

A detailed description of these modeling steps, including their implementation in COMSOL® Multiphysics and some exemplary results, is given in the following section.

3. Description of the Modeling Steps

3.1 Plasma Properties (0D)

The laser gas premix used in Rofin's DC-lasers is designed for efficient cooling and long-term stability regarding the dissociation of CO_2 into CO and O_2 without a catalytic regeneration of the gas. It consists of 6 components, listed in table 1 together with their respective functions for the discharge and the laser operation.

Each of the gas components has many different states and transitions to consider, as for example ionization and electrical, vibrational and rotational excitation. Actually, far more than 100 different electron impact reactions can occur in the discharge. According to literature and previous research, this number can be reduced by only considering the most relevant processes. However, even then 21 molecule species and 59 electron impact reactions have to be considered. The required collision cross-sections were acquired from the LXCat cross-section database [6-9].

Vol%	Gas	Function
65	He	cooling
3	Xe	(pre-)ionization
3	O_2	electron attachment
19	N_2	resonant energy transfer to CO_2
4	CO_2	lasing transition
6	CO	long-term stability

Table 1. Components of the premixed laser gas

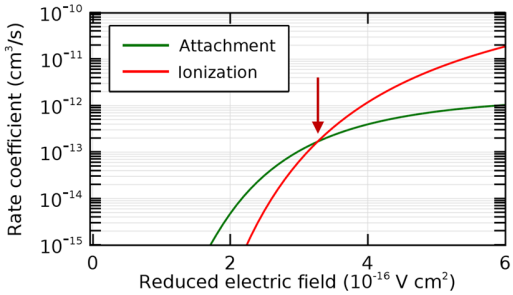

Figure 2. Ionization (red) and attachment rate (green) for varying reduced electric field. Red arrow denotes local equilibrium neglecting transport processes.

Because of the numerous species involved it is not trivial to assume a certain type (e.g. Maxwellian or Druyvesteyn) of the electron energy distribution function (EEDF) a priori. Therefore, the first step is to calculate the EEDF, the reduced transport properties and the rate coefficients for the premixed gas by use of the Boltzmann Equation, Two-Term Approximation interface in COMSOL®.

The results of this first step are used via interpolating functions in subsequent simulation steps. The calculated rate coefficients agree well with the known functions of the different gas components listed in table 1. Helium, for example, has by far the largest contribution to the elastic scattering of electrons, which corresponds to the energy diffusion in the gas (or cooling).

The discharge is locally stable, when the rate of electron production by ionization is equal to the rate of electron attachment. In a spatially distributed system, of course transport processes have to be considered as well, so that this local stability criterion is not necessarily fulfilled. However, the balance of ionization and attachment gives a first estimate for the working regime of the plasma discharge.

The sum of rates for all ionization processes and all attachment processes is shown in figure 2. The red arrow denotes the reduced electric field, at which the discharge is in equilibrium, when transport processes are neglected.

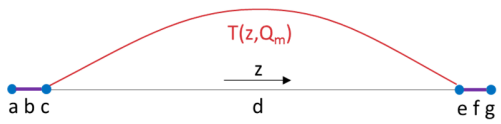

Figure 3. Illustration of the 1D discharge geometry (not to scale). Red: parabolic temperature profile. See text for further references (a-g).

3.2 Plasma Simulations (1D)

The discharge was simulated using the Capacitively Coupled Plasma interface in COMSOL®. The geometry and boundary conditions are depicted in figure 3. The one-dimensional calculation domain (a-g) is coinciding with the electrode surface normal (z-direction) and bounded by the electrode surfaces (a, g), which are coated with a dielectric material (b,f). In the regions b and f a Charge Conservation node is used along with the material properties of the dielectric coating. The plasma model, electron impact reactions and species are defined on the interval d.

The boundary conditions are set to ‘Ground’ (a) and ‘Terminal’ (g), where a prescribed current is used to ensure a unique solution (see below). Points c,e are considered to be walls, where the surface charges accumulate, and the molecules are de-ionized and de-excited using wall reactions.

A time-dependent solver is used to simulate the temporal evolution of the discharge in the gap until a quasi-steady state is reached, where the solution does not change anymore, except for the periodic variations due to the oscillation of the driving RF field.

In the following section, it will become clear that for a valid description of the discharge behavior, the gas temperature has to be self-consistent according to the heat dissipated in the discharge. Solving the plasma physics and the heat equation simultaneously would lead to very long simulation times, as the thermal time scale is some orders of magnitude slower than the plasma dynamics.

Simulations of the heat equation with a realistic heat source distribution have shown that the stationary temperature profile along the z-axis is parabolic, with a fixed temperature $T_0 = 300$ K at the electrodes (a,g). The maximum temperature is only dependent on the average heat source in the gap. Therefore, instead of solving the heat equation on the physical time scale, the temperature profile is parameterized as $T(z,Q_m)$, where Q_m is the spatially integrated heat source, averaged over a time constant τ_p in the order of 3…5 RF cycles. This artificial time scale ensures a fast convergence to the self-consistent quasi-steady state. However, it is clear that the ‘temporal’ evolution of the temperature does not reflect the physical time scale anymore, so it is not

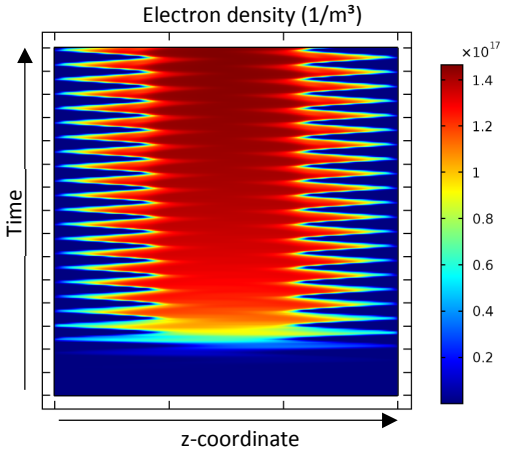

Figure 4. Spatiotemporal evolution of the electron density in the discharge gap. Left and right border of the graph coincide with lower and upper electrode.

possible to investigate the dynamics of the gas discharge.

The spatiotemporal averaging of the heat source is implemented using a global ordinary differential equation (ODE) for Q_m:

$$\frac{\partial Q_m}{\partial t} = (Q_{int} - Q_m)/\tau_P$$

where Q_{int} are the spatially integrated capacitive losses in the plasma. The nojac-operator and a segregated solver are used to decouple the temperature calculation from the plasma physics for better convergence.

Figure 4 shows an example of the spatiotemporal evolution of the electron density after switch-on of the RF power: after a few RF cycles, the discharge is ignited and the electron density raises quickly from a low pre-ionization level to a significant amount. It is visible that the electrons are following the RF oscillation almost instantaneously, while the heavy ions (not depicted) remain almost stationary. After a while (depending on the applied terminal current) the electron density and temperature settle to a quasi-stationary, periodically oscillating state.

Under the assumptions made in section 2.2 the 1D model is valid at arbitrary lateral positions in the electrode gap, but the boundary conditions depend on the local electric field. A parametric study over varying RF current amplitudes yields important result parameters, e.g. the terminal voltage (figure 5), phase angle, collision rates, or

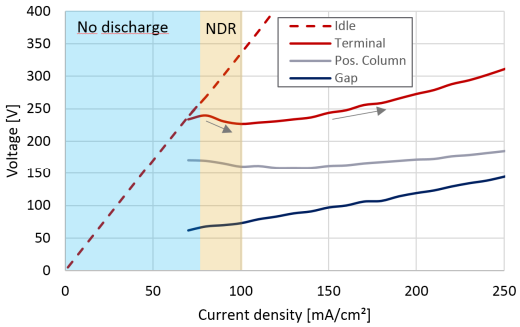

Figure 5. Discharge characteristics: voltages over applied terminal current density. Dashed: idle terminal voltage. Red: terminal voltage. Blue: voltage drop over boundary layer. Gray: voltage drop over positive column. NDR = negative differential resistance.

temperature, which can be re-substituted into the 3D simulations later.

For low current densities (blue background in figure 5) the resulting electric field is low, and the attachment rate is higher than the ionization rate (cf. figure 2), the electron density decreases over time and no discharge is ignited.

The negative differential resistance (yellow background) is a thermal effect, which is only observable with self-consistent calculation of the temperature. In this region the solution is bistable for a prescribed terminal voltage. It's an important feature of the discharge which manifests in the typical nonlinear behavior of a discontinuous ignition of the plasma above a threshold voltage.

3.3 Nonlinear Surrogate Material Model

To reproduce this behavior in spatially extended RF simulations with many degrees of freedom, a surrogate material with certain properties is required. The material model should be homogeneous and isotropic to reduce the number of required mesh elements. It must be formulated in a way that a unique solution can be found without solving a time-dependent problem. And finally the nonlinear dependencies should be sufficiently smooth to avoid convergence issues.

Figure 6 shows the geometrical setup for the surrogate material. The plasma discharge is replaced by a conductive sheet of material between the electrodes with nonlinear conductivity $\sigma_s(E(x,y))$. The conductive sheet does not fill the complete gap, but is separated from the electrodes by a (constant) distance d_s on each side.

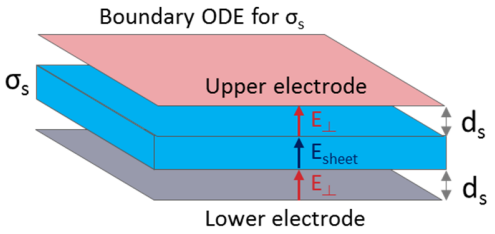

Figure 6. Illustration of the setup for the surrogate material in the 3D simulation.

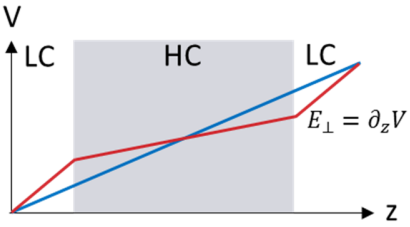

Figure 7. Illustration of ambiguous solutions regarding terminal voltage. V = electric potential. Blue: no discharge, red: with discharge (HC = high conductivity, LC = low conductivity). See text for explanation.

In figure 7, the electric potential V along the discharge gap is plotted for two exemplary solutions in the bistable region. The blue curve shows a solution without ignited plasma, and the red curve illustrates the potential distribution with plasma, where a region with high electron density (high conductivity, HC) exists in the middle of the gap, surrounded by boundary layers with low electron density (low conductivity, LC).

Both solutions have the same potential at the terminals, but the electric field or potential gradient is different. As opposed to the terminal voltage or the potential gradient in the HC region, the solution can be uniquely identified by the (normal) electric field $E_\perp$ at either electrode surface. By choosing $E_\perp$ instead of V as argument, the function σ_s is still nonlinear, but unique, monotonous and sufficiently smooth.

Furthermore, the normal electric field at the electrode surface $E_\perp$ is directly accessible in the Electromagnetic Waves interface in COMSOL®.

In order to find the matching value for d_s and the function $\sigma_s(E_\perp)$, a parametric study is performed with the Electric Currents interface in 1D, where different terminal currents are applied for several combinations of constant d_s and σ_s.

The minimum phase angle between voltage and current at the terminal only depends on d_s, which allows to determine the gap distance in a first step by matching the minimum phase angle over varying σ_s. Afterwards, an interpolation function is set up which yields the same dependency between current and voltage at the terminals as in the plasma simulations (figure 8).

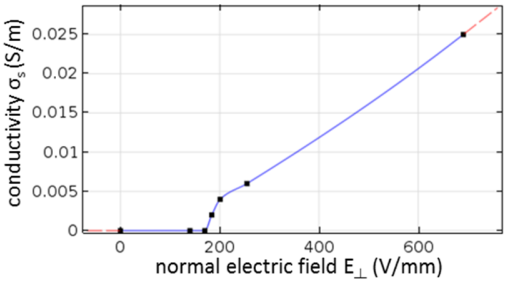

Figure 8. Interpolation function $\sigma s(E_\perp)$ used as nonlinear surrogate material model.

3.4 RF Simulations (3D)

For the macroscopic RF simulations in 3D the Electromagnetic Waves interface is used with a frequency domain solver. Due to the skin effect, it is unnecessary to include bulk metals in the calculation domain, as the skin depth is much smaller than any relevant geometrical feature of the laser for the frequency and materials used.

Therefore, the calculation domain consists only of the gas volume inside the recipient and some domains containing dielectric materials. At the metal surfaces, an impedance boundary condition is used and the respective material properties are assigned to these boundaries.

The normal electric field is evaluated at the surface of the upper electrode, and the interpolation function $\sigma_s(E_\perp)$ derived in the previous section is defined on this surface as well (the 'reference surface').

A simple boundary ODE is solved on the reference surface for the new variable σ_m with

$$\sigma_s(E_\perp) - \sigma_m = 0.$$

By defining a new variable, an iterative, segregated solver can be used to reduce the nonlocal and nonlinear coupling in the system matrix which leads to a much better convergence. The variable σ_m is made available in the plasma domain via a General Projection model coupling.

The domain between the electrodes is split into three parts according to figure 6. The middle domain is assigned to a material with the

projected conductivity from the reference boundary. All other domains are either set to the respective dielectric materials or to $\varepsilon_r = 1$, $\mu_r = 1$ and $\sigma = 0$ S/m for the gas volume outside the electrode gap.

RF power is fed into the calculation domain at a number of coaxial ports located near one of the long sides of the electrodes.

The used mesh consists of 913,564 elements, resulting in 6,737,446 degrees of freedom (DoF) to solve for. Due to the large number of DoFs a Geometric Multigrid solver is used. On a system with 8-core CPU and 256 GB RAM it took ≈ 2 hours to find a stationary solution (figure 9).

4. Results and Discussion

An example of the numerical results is shown in figure 9, where the normal current density in the electrode gap is depicted together with a representation of the surrounding structure with the upper electrode removed for better visualization. It can be seen that the discharge in this example is homogeneous within a range of about 10%.

The results have been compared to and found to agree well with experimental observations in different parameter regimes and configurations. After this verification of the modeling approach, the model has been successfully applied in subsequent development tasks, e.g. the design of a new RF feeding / matching architecture and the prediction of stable working points for alternative gas compositions.

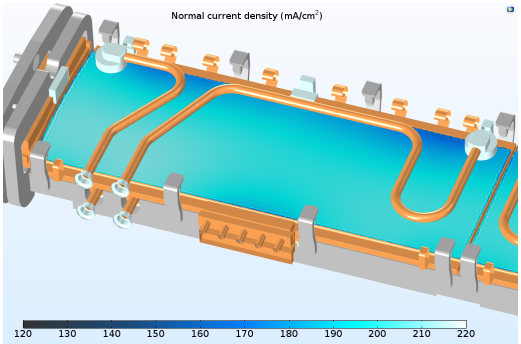

Figure 9. Current density distribution of the discharge (example)

5. Conclusions and Outlook

With the multilevel approach presented in this work it is now possible to determine the homogeneity of the discharge, power and temperature distributions, optical properties of the gas including the laser pump rates and the resulting laser gain. The RF simulations do not only provide macroscopic information, but also local information on the microscopic level via re-substitution. With these results and the available simulation tools, it is possible to identify further development potentials and to optimize our current and future products.

A future perspective is to extend the model with respect to the transient spatiotemporal behavior during the ignition of the plasma. This would allow to investigate e.g. pressure variations during switch-on of the laser and to further optimize the performance of the laser in pulsed operation.

6. References

1. W. Rath et al., Industrial Laser Materials Processing, *Laser Technik Journal*, **11**, 23–27 (2014)
2. R. R. Nowack et al., High-power CO_2 waveguide laser of the 1-kW category, *Proc. SPIE*, **1276**, 18 (1990)
3. R. Wester, *Hochfrequenzgasentladungen zur Anregung von CO_2-Lasern*, Dissertation, RWTH Aachen (1987)
4. P. P. Vitruk, et al., Similarity and scaling in diffusion-cooled RF-excited carbon dioxide lasers, *IEEE Journal of Quantum Electronics*, **30(7)**, 1623-1634 (1994)
5. J. Schulz, *Diffusionsgekühlte, koaxiale CO_2-Laser mit hoher Strahlqualität*, Dissertation, RWTH Aachen (2001)
6. Morgan database, www.lxcat.net, retrieved on January 12, 2016.
7. Hayashi database, www.lxcat.net, retrieved on January 22, 2016.
8. Itikawa database, www.lxcat.net, retrieved on January 22, 2016.
9. Biagi-v8.9 database, www.lxcat.net, retrieved on August 19, 2015.